

Coulomb Stress Failures in Fracture Networks Resulting from Hydraulic Fracturing: A Tutorial

Kris Vasudevan* and David W. Eaton
Department of Geoscience, University of Calgary
vasudeva@ucalgary.ca

Summary

In hydrocarbon-producing sedimentary basins, the crust behaves as a poroelastic medium. The empirical Coulomb failure criterion is applicable to this medium. The stress state of the poroelastic medium, which entails both the shear and normal stress of the rock, is influenced by the pore fluid diffusion. Coulomb stress changes due to pore pressure changes in a poroelastic medium lead to microseismic events. This is also true of any hydraulic fracturing where the fluid injection changes the pore pressure and hence, changes in the mean stress of the medium. Despite the fact that the poroelastic dynamics is highly complex even with homogeneous properties, understanding the physical process of pore-fluid induced microseismicity is critical to planning and carrying out successful hydraulic fracturing experiments. In this tutorial, we introduce the concept of Coulomb stress failure changes as applied to the study of regional static stress changes in tectonically active earthquake areas causing spatially predictable aftershocks. We consider the reasons to think beyond the double-couple mechanism as a source characteristic for microseismicity due to hydraulic fracturing. Finally, we propose a complex network model of microseismic events with every event caused by pore fluid relaxation subsequent to a pore-pressure change so that a time-dependent, composite Coulomb stress failure map of the medium under modified stress is realizable.

Introduction

Coulomb stress failure changes have been extensively studied in the context of earthquakes where the source mechanism is exclusively dominated by double-couple forces. For reasonably well-estimated moment tensors from the measured three-component waveforms at many seismic stations favorably located in the vicinity of earthquake prone areas, automated methods are now available to compute the Coulomb stress failure maps. Such maps are routinely generated for earthquakes on strike-slip faults, normal faults, and reverse faults. The maps contain both positive and negative stress failure regions with positive regions spatially designated as regions of aftershocks. The importance of pore pressure changes subsequent to earthquakes in releasing fluids along faults and fractures, and in the spatial distribution of aftershocks in actively tectonic zones has been the subject of research studies in recent years. Not surprisingly, what has been observed for large earthquakes is found to hold good for microseismic events and their aftershocks.

It is becoming a common industry practice to collect microseismic data from either one or many observation wells with a multiple array of sensors. Aside from real challenges in accurately locating the event locations, there are issues that are to do with establishing the source mechanisms of the events. The accuracy of the location information is much sought after particularly when only one observer well is present and the velocity information of the invaded formation from the injected fluid is not fully factored into any travel-time procedures. Despite these challenges, rapid strides in advancing accurate determination methods are

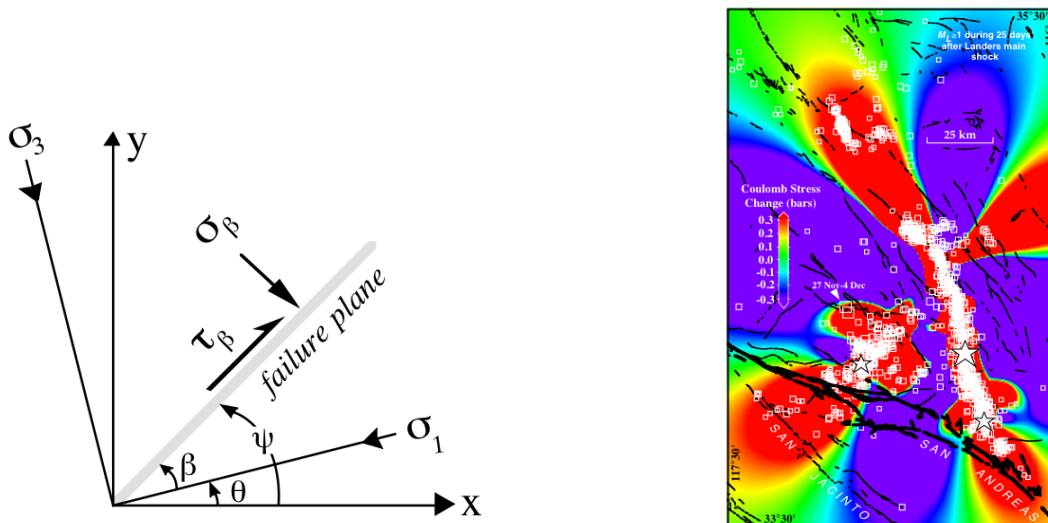
being made. Aside from the commonly understood and accepted double-couple slip mechanisms for the occurrence of microseismic events in a hydraulic fractured medium, the role of compensated linear vector dipole and the isotropic tensor components is being stressed in recent studies. In this tutorial, we visit the topic of Coulomb stress failure changes as has been applied to strike-slip fault earthquakes in predicting the spatial distribution of aftershocks. Against this background, we consider the pore pressure changes of fluids on aftershocks in tectonically active regions and in creating earthquake swarms upon injecting fluid into a formation to enhance oil/gas production in a sedimentary basin. We point out the growing role of a weighted moment tensor solution with double couple, non-double couple and volumetric components.

Theory and Method

The Coulomb failure criterion is commonly used to characterize failure in rocks. Both the shear and normal stress on a preexisting or an incipient fault plane satisfy conditions analogous to those of friction on a preexisting surface. When the Coulomb stress, also referred to as Coulomb failure function, exceeds a specific value,

$$CFF = \tau_{\beta} + \mu (\sigma_{\beta} + p)$$

where τ_{β} is the shear stress on the failure plane, σ_{β} is the normal stress (positive for extension and negative for compression), p is the pore fluid pressure, and μ is the coefficient of friction, failure occurs on the plane (Figure 1, left). Certain modifications to the above equation have been suggested for cases where rock stress is changed more rapidly than fluid pressure can change through flow. In a system where the x- and y-



Adapted from King, Stein, and Lin, *Bull. Seism. Soc. Am.* (1994)

Figure 1: (left) The axis system used for Coulomb stress (after King, Stein and Lin, BSSA, 1994); (right) The largest Coulomb stress changes at depths between 0 and 12.5 km caused by the Landers, Big bear and Joshua Trees earthquakes with the first 25 days of seismicity. Also shown are the largest two aftershocks to occur during the following 8 months, the November 17, 1992 ($M_L = 5.3$) and December 4, 1992 ($M_L = 5.1$) shocks (from King, Stein and Lin, BSSA, 1994)

axes and fault displacements are horizontal and fault planes are vertical (z-axis), stress on a plane at an angle ψ from the x-axis (see Figure 1) is

$$\begin{aligned} \sigma_{11} &= \sigma_{xx} \cos^2 \psi + 2\sigma_{xy} \sin \psi \cos \psi + \sigma_{yy} \sin^2 \psi \\ \sigma_{33} &= \sigma_{xx} \sin^2 \psi - 2\sigma_{xy} \sin \psi \cos \psi + \sigma_{yy} \cos^2 \psi \\ \tau_{13} &= \frac{1}{2} (\sigma_{yy} - \sigma_{xx}) \sin 2\psi + \tau_{xy} \cos 2\psi \end{aligned}$$

For example, the Coulomb stress for a right-lateral motion on planes orientated at ψ with respect to the x -axis is

$$\sigma_f^R = \tau_{13}^R + \mu' \sigma_{33}$$

King, Stein and Lin (1994) have successfully applied the static Coulomb stress failure changes for any earthquake event where the source characteristics for a given moment magnitude are known from well-established moment tensor inversion methods. Figure 1 (right) illustrates one example where they have demonstrated the usefulness of their method in identifying the spatial locations of aftershocks of earthquakes with the positive Coulomb stress failure changes.

Models

For the hydraulic fracturing experiment, we consider the approach of Sibson (1997) to be valid. As shown in Figure 2 (left), the formation rock is made up of layers of inter-linked “meshes” subsequent to hydraulic fracturing. For such a scenario, we use the Coulomb stress failure condition, as represented by the Mohr diagram (Figure 2 (right)). We look upon the red-hashed area within each mesh as being representative of the rupture geometry. What combination of double couple, non-double couple, and volumetric forces would emulate this is not an easy problem. The generality of the mesh model is appealing since the embedded features in them can be easily incorporated into a complex network model for a study of the fluid-induced fractures, recently suggested by Vasudevan and Eaton (2010).

Hill (1977) mesh model for earthquake swarms

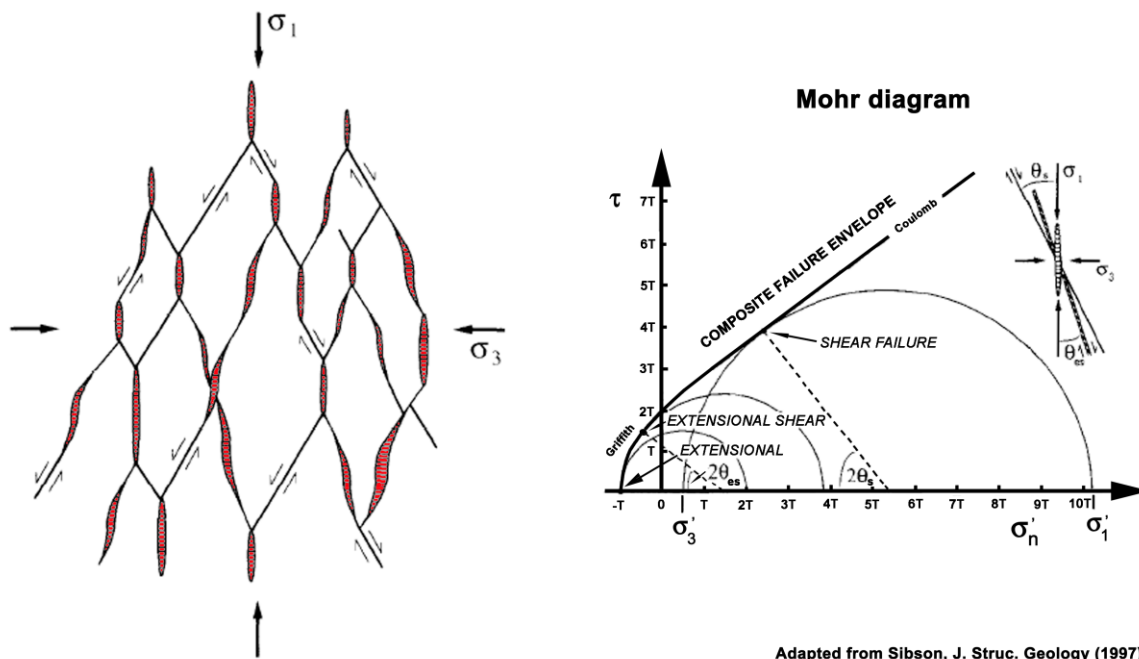
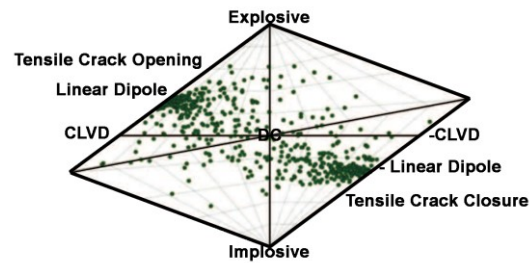
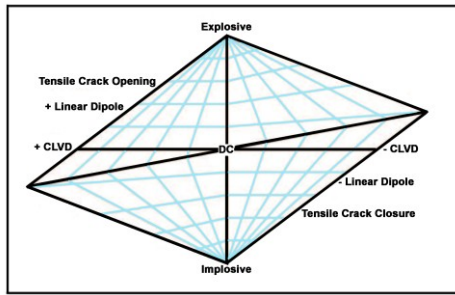


Figure 2: (left) A model comprising shear, extensional, and extensional-shear fractures developed. This one diagram could represent an extensional normal-fault stress regime when upright, a compressional thrust-fault regime when viewed sideways, and a strike-slip regime in plan view; (right) Mohr diagram with composite failure envelope for intact rock with tensile strength, T.

In spite of the challenges, attempts have been made to use source-type diagrams (See Figure 3), with them populated with microseismic events satisfying certain hybridization of all different types of forces contributing to the source mechanism (Hudson et al., 1989; Baig and Urbancic, 2010). We consider in this tutorial how we deal with the generation of time-dependent Coulomb stress failure maps.



Adapted from Baig and Urbancic, *The Leading Edge* (2010)

Figure 3: (left) A source-type diagram for microseismic events in a hydraulic fracturing experiment. A microseismic event with a hybrid source mechanism comprised of double-couple, compensated linear vector dipole, and isotropic contributions to the moment tensor enters as a point in this diagram; (right) A source-type diagram for one treatment in a well from a field

Conclusions

Understanding the conditions under which Coulomb stress failure changes in a brittle crust under the influence of pore pressure changes of the injected fluid become positive is important.

The crust in hydrocarbon producing sedimentary basins is under stress even in its undrained state of the pores. Whether or not the formations have naturally occurring fractures and faults, any increase in pore pressure means an increased resistance to normal forces. When the shear stress failure criteria are met, slip will occur on the existing fractures and faults or new fractures will form. Usually, these new fractures are oriented in the regional stress field. For a fluid injection along the minimum shear stress direction, i.e. the least principal stress axis, fractures appear in a direction perpendicular to this, i.e. along the greatest principal stress axis.

With meaningful complex network models and Coulomb stress failure maps, it is possible to analyze the dynamics of hydraulic fracturing in formations. Since we go from one event scenario to a case of multiple events, we need to examine the statistics of the underlying processes and also, provide the degree of uncertainty in the answers we seek.

Acknowledgements

The authors would like to acknowledge the Natural Sciences and Engineering Research Council of Canada for financial support.

References

- Baig, A., and Urbancic, T., 2010, Microseismic moment tensors: A path to understanding frac growth: *The Leading Edge*, 320-324.
- Barnhoorn, A., Cox, S.F., Robinson, D.J., and Senden, T., 2010, Stress-and fluid-driven failure during fracture array growth: Implications for coupled deformation and fluid flow in the crust: *Geology*, 38(9), 779-782; doi: 10.1130/G31010.1
- Bosl, W.J., and Nur, A., 2002, Aftershocks and pore fluid diffusion following the 1992 Landers earthquake: *J. Geophys. Res.*, 107(12), No. B12, 2366; doi: 10.1029/2001JB000155.
- Hickman, S., Sibson, R., and Bruhn, R., 1995, Introduction to special section: Mechanical involvement of fluids in faulting: *J. Geophys. Res.*, 100, 12,831-12,840; doi: 10.1029/95JB01121.
- Hudson, J., Pearce, R., and Rogers, R., 1989, Source type plot for inversion of the moment tensor, *J. Geophys. Res.*, 94, 765 – 774.
- King, G.C.P., Stein, R.S., and Lin, J., 1994, Static stress changes and the triggering of earthquakes: *Bull. Seism. Soc. Am.*, 84(3), 935-953.
- Maxwell, S.C., Rutledge, J., Jones, R., and Fehler, M., 2010, Petroleum reservoir characterization using downhole microseismic monitoring: *Geophysics*, 75(5), 75A129-75A137.
- Okada, Y., 1985, Surface deformation due to shear and tensile faults in a half-space, *Bull Seism. Soc. Am.*, 75(4), 1135-1154.
- Sibson, R.H., 1997, Structural permeability of fluid-driven fault-fracture meshes: *J. Struct. Geology*, 18, 1031 - 1042.
- Urbancic, T.I., Trifu, C-I., and Young, R.P., 1993, Microseismically derived fault-planes and their relationship to focal mechanism, stress inversion, and geologic data, *Geophys. Res. Lett.*, 20, 2475 – 2478.
- Vasudevan, K., and Eaton, D. W., 2010, Complex network model and Coulomb stress failure changes, Unpublished results.
- Vavrycuk, V., Bohnhoff, M., Jechumtalova, Z., Kolar, P., and Sileny, J., 2008, Non-double-couple mechanisms of microearthquakes induced during the 2000 injection experiment at the KTB site, Germany: A result of tensile faulting or anisotropy of a rock?: *Tectonophysics*, 456, 74 - 93.